COBEM 2023 27TH INTERNATIONAL CONGRESS OF MECHANICAL ENGINEERING

ABCM Brazilian Society of Mechanical Sciences and Engineering
27th ABCM International Congress of Mechanical Engineering
December 04-08, 2023, Florianópolis-SC, Brazil

COB-2023-1770
CALCIUM CARBONATE PRECIPITATION IN PERFORATED LINERS: A COMBINED THERMODYNAMIC, KINETIC AND CFD MODELING APPROACH

Vinicius Gustavo Poletto
Thiago Machado Neubauer
Marina Elizbeth Mazuroski
Fernando Cesar De Lai
Silvio Luiz de Mello Junqueira
Research Center for Rheology and Non-Newtonian Fluid (CERNN) | Federal University of Technology – Parana (UTFPR)
vinsptt19@gmail.com
thiagoneubauereq@gmail.com
marina.mazuroski@gmail.com
fernandodelai@gmail.com
silvio@utfpr.edu.br

Bruno Barbosa Castro
Helga Elizabeth Pinheiro Schluter
Andre Leibsohn Martins
Leopoldo Américo Miguez de Mello Research (CENPES) | Petrobras
bbcastro@petrobras.com.br
helga@petrobras.com.br
aleibbsohn@petrobras.com.br

Abstract. *The calcium carbonate formation represents a financial and technological challenge for the oil and gas industries, since it may lead to serious flow assurance issues. The mathematical prediction of the precipitation rates produced along the oil and gas downhole completion is a useful tool for risk management during the well project stage. A mathematical methodology involving the calcium carbonate thermodynamic, kinetics, and flow dynamics along the production flow line is developed. The proposed simulation workflow combines a polymorphic populational model to define the CaCO3 particles kinetics, a multiphase thermodynamic model to simulate the supersaturation conditions, and computational fluid dynamics to produce the pressure and velocity profiles of each equipment of the completion configuration. Combining simulation of the three models results in kinetic and thermodynamic precipitation rates. The developed mathematical workflow is applied to an open-hole 3-zone completion assembled with a 300m perforated tube with ½" holes. The completion operates with pressures, temperature, and salinities up to 450 Bar, 64°C, and 5 mol. L-1. The results indicate increasing precipitation rate, for both kinetic and thermodynamic ones, along the upstream direction. Notably, the kinetic rate produced a value in the range of mgCaCO3/day instead of the kgCaCO3 of the thermodynamic simulation. Besides that, it is possible to observe the influence of the pressure and residence times leading to an increase severity upstream the completion.*

Keywords: *Calcium Carbonate, Inorganic Scaling, Flow assurance, Well completion, Population balance*

1. INTRODUCTION

The formation and deposition of inorganic salts on industrial equipment surfaces pose significant financial and technological challenges for various industries, particularly the oil industry, due to the transportation of multiphase fluids such as water, oil, and gas under high temperature, pressure, and salinity (Crabtree, M., Eslinger, D., Fletcher, P., Miller, M., Johnson, A., King, 1999; Kamal et al., 2018a). These conditions can bring significant challenges in scale control, especially for calcium carbonate scaling, which is a scale type that can be vulnerable to pressure and temperature variations (Blue et al., 2017; Cosmo, 2013a; Du & Amstad, 2019). To ensure optimal production control and scale surveillance, smart completions are considered one of the most favorable methods, as they allow for the reduction of water production or the mixing of incompatible water chemistries (Bouamra et al., 2020; H. F. L. L. Santos et al., 2017). However, the design, size, and geometry of the smart completion tool can impact the prevention of scaling deposition. As a result, there is a need to investigate operating conditions and equipment design that can promote the formation and deposition of precipitates within the oil production process (Kamal et al., 2018a; Sanni et al., 2022). To address this issue, a mathematical methodology has been developed that predicts precipitation rates along the oil and gas workflow within

these smart completions. A complete simulation of the particles, characterizing the kinetic, thermodynamic, and fluid-dynamic aspects of the $CaCO_3$ produced within the fluids produced in the oil and gas industry, could be used as a virtual sensor for potential analysis, control and monitoring of incrustation problems, offering a more complete tool than the pure thermodynamic simulations that are usually used as prediction tools by the oil and gas industry (Bouamra et al., 2020; Lassin et al., 2018; T. Neubauer et al., 2022; Sanni et al., 2015). The proposed methodology involves the use of calcium carbonate thermodynamics, kinetics, and flow dynamics along the production flow to assess the risk of $CaCO_3$ precipitation. The simulation workflow combines a polymorphic population model to define the $CaCO_3$ particle kinetics, a multiphase thermodynamic model to simulate supersaturation conditions, and computational fluid dynamics to produce the pressure and fluid flow profiles of the completion. The combined simulation of the three models produces kinetic and thermodynamic precipitation rates. This work describes the model calculations to assess calcium carbonate formation in an open-hole completion assembled with a perforated liner composed of multiple tiny, drilled holes along the production tubing.

The formation and deposition of calcium carbonate precipitates are known to be influenced by various factors, including supersaturation, temperature, pH, calcium and bicarbonate/carbonate ratio, CO_2 pressure, and the presence of external ions (Blue et al., 2017; Cosmo, 2013; Haarberg et al., 1992; Olajire, 2015). Additionally, the formation of metastable forms as intermediates in the formation of a more stable form is also dependent on these factors, especially the water content (Donnet et al., 2009; Du & Amstad, 2019). Many studies have used these fundamental concepts to model the calcium carbonate formation under different experimental or theoretical conditions, including high temperature and pressure, standard temperature and pressure, and multiphase systems (Brečević & Kralj, 2008; Cosmo, 2013; Myasnikov et al., 2013; T. M. Neubauer, 2022). The thermodynamics of calcium carbonate formation are primarily concerned with two aspects: the calculation of supersaturation under aqueous solution conditions, and the energy profile of the forms to predict their stability and likelihood of precipitation. Several models have been developed based on this approach to simulate calcium carbonate formation, some of which are now commercially available, like Multiscale® (Expro Petrotech, 2023) and PhreeQC (U.S Geological Survey, 2023).

The study of the kinetic aspect of calcium carbonate formation is diverse, encompassing individual rates under varying conditions and polymorphs, rate-limiting steps, polymorphic transformation, velocity, and mechanisms among different phases and external ions. However, despite significant progress, the complexity of the underlying mechanisms involved in calcium carbonate formation is still not fully comprehended (Lassin et al., 2018; Myasnikov et al., 2013; T. Neubauer et al., 2022; Sanjiv Raj et al., 2020). Kinetic models may be seen as further improvement in the calcium carbonate precipitation modelling, although its results can differ significantly from thermodynamic models; as exemplified by the work of (Hamid et al., 2013) that developed and applied a kinetic model to predict blockage time in tube-blocking tests and obtained very different results when applying the pure thermodynamic or kinetic model.

Compared to the thermodynamic aspect, there have been relatively few kinetic studies on the precipitation of calcium carbonate under oil and gas industry conditions (Myasnikov et al., 2013; T. M. Neubauer, 2022; Sanni et al., 2022). While the tool for calculating supersaturation has been extensively studied and validated for these conditions, the same is untrue for the calcium carbonate populational kinetics (Du & Amstad, 2019; Gebauer et al., 2018; Olajire, 2015). However, it is important to notice that the difficulty in obtaining data from systems with high temperature, pressure, and salinity is a major limitation to the quality of both thermodynamic and kinetic parameters (Gebauer et al., 2018; Kawano et al., 2009; Van Driessche et al., 2017). Despite these challenges, researchers have shown great interest and effort in continually developing tools that can provide a different approach or conclusion to this topic (Du & Amstad, 2019; Kamal et al., 2018; Mayorga et al., 2019; Olajire, 2015). In this work, a novel approach involving fluid dynamic, thermodynamics and kinetics is presented to evaluate the calcium carbonate precipitation potential in a an open-hole completion assembled with a perforated liner. Such results outlook a robust and phenomenological approach to a multi-disciplinary and challenging problem for flow assurance.

2. METHODOLOGY

The present topic proposes a methodology for calcium carbonate formation in a completion assembled with perforated liner identified as PACS3A. The simulation model involves solving fluid dynamics, thermodynamics of phase equilibrium, and kinetics of particle populations. The simulation workflow described in detail in the following sections comprises 5 steps.

- Step 1: estimation of bulk averaged fluid properties under downhole conditions;
- Step 2: computation of boundary conditions to characterize the production into each configurated considered;
- Step 3: conception of the geometry and simulation domain of completions tools that compose the configurations;
- Step 4: simulation of one-phase, steady-state, and turbulent flow for calculation of velocity and pressure profiles;
- Step 5: population balance simulation in terms of the water composition, pressure profile and velocity profile to compute CaCO3 precipitation rates along the completion.

2.1 CFD: velocity and pressure profiles

The CFD approach involves the following steps:

- Fluid properties and boundary conditions determination;
- Completion equipment geometry and fluid domain conception;
- Mesh generation in fluid domain;
- Turbulent one-phase fluid flow simulation;
- Results compilation with velocity magnitude and pressure profile computation for the entire open-hole region.

The computation of fluid properties follows the assumption that there is only water and oil flowing in downhole conditions. The gas phase, in this sense, supposedly is fully dissolved in either one of the phases. The total flow rate Q_{total} [bbl/d], considered as reference, comprises the sum of the water flow rate Q_{water} [bbl/d] and oil flow rate Q_{oil} [bbl/d], as listed in Table 1. Both flow rates are corrected for downhole thermodynamic conditions considering a pressure of 335 bara and 62ºC and oil volume formulation factor measured by PVT-testing samples.

Table 1 – Reference flow rate Q_{total} [bbl/d] comprises the sum of the water flow rate Q_{water} [bbl/d] and oil flow rate Q_{oil} [bbl/d] assuming that the gas phase remains fully dissolved in downhole condition.

Q_{water}	637	m^3/d	$4.005\ 10^3$	bbl/d
Q_{oil}	5673	m^3/d	$3.568\ 10^4$	bbl/d
Q_{total}	6310	m^3/d	$3.968\ 10^4$	bbl/d

Fluid Properties evaluated by PVT testing for water and oil listed in Table 2 are averaged to represent equivalent properties of a water-oil emulsion. For the sake of modeling and simulating, the CFD runs turbulent equations for a one-phase flow. Considering the flow rate listed in Table 1, it is reasonable to assume that there is no slippage in the water-oil interface. In this sense, the water-oil equivalent specific mass $\rho_{w/o}$ [kg/m^3] is averaged in terms of water and oil volumetric fraction. The water-oil equivalent viscosity $\mu_{w/o}$ [Pa.s] follows Taylor (1932) expression.

Table 2 – Fluid properties computed in terms of the equivalent water-oil specific mass $\rho_{w/o}$ [kg/m^3] and apparent viscosity $\mu_{w/o}$ [Pa.s] for the simulation of the one-phase turbulent flow. The calculation of equivalent properties depends on the properties of the oil and water phase corrected for the downhole thermodynamic conditions of 335 bara and 62ºC.

Oil specific mass	ρ_o	667.8	kg/m^3
Oil viscosity	ρ_w	$7.6640\ 10^{-4}$	Pa.s
Water specific mass	μ_w	934.8	kg/m^3
Water viscosity	μ_o	$2.13.10^{-4}$	Pa.s
Water-oil equivalent specific mass	$\boldsymbol{\rho_{w/o}}$	**695**	$\boldsymbol{kg/m^3}$
Water-oil equivalente viscosity	$\boldsymbol{\mu_{w/o}}$	$\boldsymbol{8.663\ 10^{-4}}$	**Pa.s**

The scope of the present work is the PACS 3A configuration, as depicted in Figure 1 (a) consisting of tree production zones in open-hole configuration, namely inferior, intermediate and superior. Between each zone, there is a 20.6m packer. A perforated liner with 30 holes of ½" per meter spread across each zone. At this point, it would be necessary to address how each zone contributes to the total flow rate Q_{total}, computed in Table 1. In the perforated linear completion scenario, it would be very difficult to measure the individual flow rate of each zone, also available data in the literature is scarce. In this sense, considering the lengthily perforated liner, it is reasonable to assume that the flow rate is evenly distributed in the well wall, being proportional to the zone length. In such scenario, the inferior zone produces 12860 bbl/d across 143.3 m, the intermediate produces 11890 bbl/d across 132.5 m, and the superior zone produces 14930 bbl/d across 166.4 m, as indicated by Table 3. Figure 1 (b) depicts a schematic representation of the flow rate distribution in the PACS 3A configuration, note that the flow rate increases inside the perforated liner from the bottom hole (upstream) towards the top of the open-hole region (downstream) as each ½" hole delivers a fraction of the total flow rate.

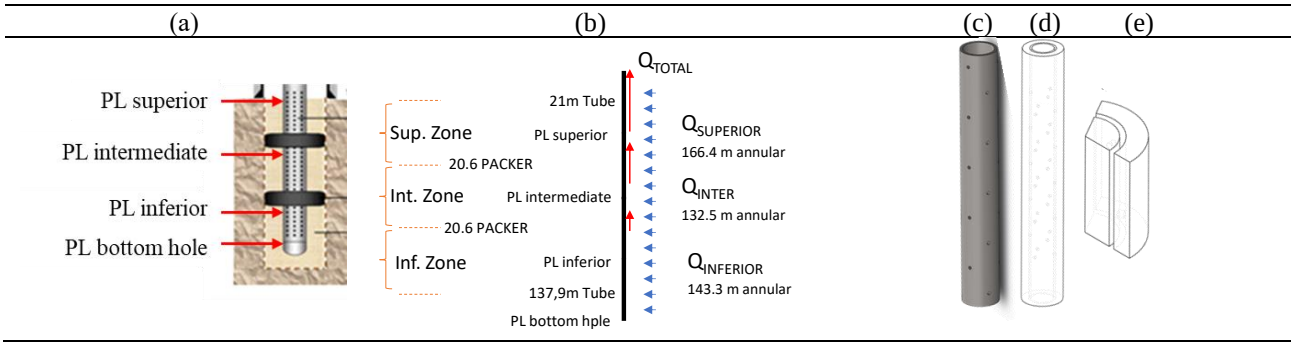

Figure 1 – Open-hole completion assembled with perforated liner: (a) schematic representation of inferior, intermediate and superior production zone demarcation by packers; (b) packer location and flow rate uniform distribution as a function of length; (c) 1-m long perforated liner; (d) 1-m long fluid domain comprising an 8 ½" wellbore, and (e)) representative volume employed for simulation with 200 mm in length and 120º angular symmetry.

Table 3 – Flow rate distributed as a function of production zone length.

	Length [m]	**Main equipment**	**10^4Q [bbl/d]**
Superior zone	166.4	Perforated liner	1.493
Packer	20.6	Duct	
Intermediate zone	132.5	Perforated liner	1.189
Packer	20.6	Duct	
Inferior zone	143.3	Perforated liner	1.286

Figure 1 (c) shows a schematic representation of a 1-meter segment of the perforated liner, each hole is ½" in diameter, with a hole density of 30 holes/m. The fluid domain is bounded by an 8 ½" open-hole wellbore, as shown in Figure 1 () by the 1-m segment of the fluid domain. As discussed over the completion scheme depicted in Figure 1 (a), the perforated liner stretches all across each production zone. Supposing that the perforations are regularly distributed along each meter, it is possible to delimitate the fluid domain to a representative volume, as depicted in Figure 1 (e). The representative volume is 200-mm long and has a 120º angular symmetry. Boundary conditions properly applied in section planes represents all the extent of the flow inside the completion, as listed below.

The CFD approach considers the following assumptions:

- Fully turbulent flow, spite of the flow in annular region of REV is transitional, the most significant pressure drop is inside the column, as outlined soon;
- Isothermal flow, meaning that thermal effects are not relevant for the residence time of fluid inside the open-hole completion;
- Incompressible flow, also considering the gas phase remain fully dissolved
- Newtonian fluid with uniform viscosity, as the flow rate is high and the flow is turbulent;
- One-phase flow with equivalent-properties computed in terms of volume fraction-averaged properties of water and oil in downhole conditions;
- Isotropic turbulence, as the perforated liner is symmetrical in 120º at each 200mm, rotational effects are not relevant.

The turbulence modeling is by the means of RANS equations, employing specifically the k-ε realizable model proposed by Shih et al. (1995). Such model is widely used in commercial CFD packages, and consists of a mass balance equation and a momentum balance equations written in terms of an eddy viscosity μ_{eff} [Pa.s]. The eddy viscosity is computed by the Boussinesq approximation as a function of the turbulent intensity and the turbulence dissipation rate. The set of equations for the k-ε realizable model require suitable boundary conditions applied in the representative volume depicted in Figure 1 (e) to portrait the flow in the entire completion system, which is 486,4 m long. Boundary conditions are listed and exemplified in Figure 2.

Noteworthy, as outlined previously, the flow rate inside the perforated liner, in the column, increases upwards as each hole delivers a fraction of the total flow rate. In this sense, for the characterization of the completion system it is necessary to simulate individual and discrete domains. As marked in Figure 1 (a), it is considered representative volumes placed:

- PF bottom hole: all the downhole to capture the pressure difference between the well wall and the outlet;
- PF inferior: close to the inferior-intermediate packer to capture the pressure and velocity profiles along the axis to characterize the production of the inferior zone;

- PF intermediate: close to the intermediate-superior packer to capture the pressure and velocity profiles along the axis to characterize the combined production of the intermediate and inferior zone;
- PF superior: close to the packer sealing of the superior zone to capture the pressure and velocity profiles along the axis to characterize the total flow rate output;

Flow rate considered for CFD simulation comprises Q_{total} (39690 bbl/d) listed in Table 1 as reference with water-oil equivalent properties for one-phase flow computed in Table 2. Following the assumption of evenly distributing the flow rate as a function of zone length, as in Table 3, and the boundary conditions indicated in Figure 2, Table 4 lists the area-averaged velocity for each flow rate scenario applied in the well wall and also in the column inlet.

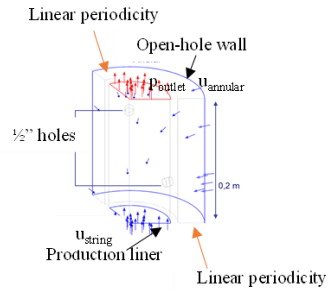

- 120º angular section plane: symmetry;
- 200-mm transverse annular section plane: linear periodicity;
- Outer annular well (well wall): area-averaged uniform velocity as a consequence that the total flow rate Qtotal supposedly evenly distributed all across the well wall;
- Column inlet: fully-developed fully-turbulent velocity profile, 5% turbulent intensity and diameter as mean length.
- Column outlet: uniform pressure;
- Perforated liner wall: no slip condition.

Figure 2 – Boundary conditions applied to the representative volume.

Table 4 – Flow rate scenarios in terms of the total flow rate Q_{total} and area-averaged velocities magnitudes employed for boundary conditions.

Zone indication		Inferior		Intermediate	Superior
Perforated tube position		PF1	PF2	PF3	PF4
$1.0Q_{total}$	10^{-2} Q_{zone} [m³/s]		2.367	2.188	2.748
	10^{-3} $u_{annular}$ [m/s]	4.511	4.511	4.511	4.511
	u_{string} [m/s]	0	2.167	4.187	6.725

2.2 Thermodynamic calculation

The first step in thermodynamic calculations is to know the initial conditions to which the phases are subjected. For this, it was considered that the completion is submerged in a well with conditions presented in Table 5.

Table 5 – Thermodynamic conditions at the selected well.

Sodium [ppm]	41.968	Sulfate [ppm]	95
Potassium [ppm]	1.751	Bicarbonate [ppm]	2.117
Magnesium[ppm]	715	pH	5,1
Calcium [ppm]	4.390	mol CO_2 [%]	16
Barium [ppm]	33	Temperature [ºC]	64
Chloride [ppm]	1.360	Pressure [bar]	415.3
Bromide [ppm]	75.902	BSW(%)	13.3%

To begin populational simulations, is necessary to ascertain the supersaturation ratio for each volume and polymorph within the conditions of Table 1. This ratio is then used to determine the deviation from chemical equilibrium (as per Equation 1), which enables an assessment of whether precipitation is required to attain a new equilibrium state. This, in turn, helps to determine the thermodynamic potential for $CaCO_3$ formation within a multiphase aqueous system.

$$SS = \frac{a_{Ca^{2+}}\, a_{HCO_3^{2-}}^{2}}{K_{eq}\, a_{CO_2}\, a_{H_2O}} \tag{1}$$

The K_{eq} calculation utilized the methodology developed by T. M. Neubauer (2022b) to determine the global equilibrium constant, K_{eq}, for the various forms of calcium carbonate under conditions of up to 200 atm pressure, 100 ºC temperature, and salinities up to 8 mol/L of NaCl. The activity and fugacity of the species present were computed using semi-empirical equations developed by Harvie et al. (1984), Lassin et al. (2017), and Pitzer & Mayorga (1973), as well as the semi-empirical methodology of Duan et al. (2006).

Using the supersaturation values of each potential polymorph, it becomes feasible to compute the quantity of calcium and bicarbonate ions required to precipitate to achieve equilibrium in the system. As a result, the potential for calcium carbonate formation can be determined as a function of temperature, pressure, CO_2 content in the gaseous phase, and salinity of each system.

2.3 Kinetic calculation

Using the thermodynamic calculations, it becomes feasible to simulate the kinetic behavior of particles through population balances. However, to apply the predictive ability of the population model to data at elevated pressures and temperatures, Neubauer's (2022) methodology can be modified to resolve systems at pressures of up to 415 atm and temperatures of up to 70 ºC, in the presence of turbulence and mixing salt currents. Given that the flow system under investigation includes an oil phase and various regions with distinct conditions, the model must take into account new considerations and hypotheses to predict the kinetics of $CaCO_3$ precipitation.

- The effect of the oil phase was considered only in the phase balance, not considering the kinetic effects that these may cause in the system;
- There is no incrustation, every formed particle flows along the system with a velocity equal to the flow;
- The activation energies of nucleation, growth, dissolution, agglomeration and transformation can be taken from (Brečević and Kralj, 2008; Myasnikov et al., 2013);
- Calcium carbonate particles present a gypsum-like agglomeration kernel (Livk & Ilievski, 2007);
- The kinetic effects that divalent ions, Mg^{2+}, Ba^{2+} and Sr^{2+} show on calcium carbonate kinetics can be represented by the empirical equations presented in (Neubauer et al., 2022);
- The equilibrium constants, adjusted up to 200 atm and 100 ºC, can be extrapolated up to 415 atm;
- For this, Equations 2 to 4 are formulated to represent the phenomenon of particle precipitation for each control volume studied.

$$\frac{dN_1}{dt} = \frac{-N_1}{2w_1} G(L_1) + B_n - A_{D,1} - kN_1{}^{ro} + \frac{Q_{in}N_{1,in} - Q_{out}N_{1,out}}{V} \quad (2)$$

$$\frac{dN_i}{dt} = \frac{-N_i}{2w_i} G(L_i) + \frac{N_{i-1}}{2*w_{i-1}} G(L_{i-1}) + A_{B,i} - A_{D,i} - kN_i{}^{ro} + \frac{Q_{in}N_{1,in} - Q_{out}N_{1,out}}{V} \quad (3)$$

$$\frac{dN_{nc}}{dt} = \frac{N_{nc-1}}{2w_{nc-1}} G(L_{nc-1}) + A_{B,nc} - kN_{nc}{}^{ro} + \frac{Q_{in}N_{1,in} - Q_{out}N_{1,out}}{V} \quad (4)$$

For this set of equations, the following parameters are considered:

- N - number of particles per m³ with size within the class, 1 for the first, i for intermediate classes and nc for the largest size class;
- w - size difference between class boundaries;
- L - upper class limit;
- G - crystal growth term;
- A_b and A_d – terms of appearance and disappearance of crystals of the class;
- K - kinetic constant of the polymorphic transformation
- ro - order of this reaction rate;
- Q_{in} and Q_{out} - volumetric flows at the inlet and outlet of the control volume; and finally,
- $N_{i,in}$ and $N_{i,out}$- number of particles with size i that enter and leave the control volume region.

Different polymorphs exhibit varying thermodynamic stabilities and reactivity; hence the model parameters were estimated based on experimental data for each polymorph and presented in Neubauer (2022). This methodology allows for the simulation of the kinetic process and the calculation of the mass of crystals per cubic meter as a function of time for the completions, using the following inputs:

- The volumetric flow of each phase present in the flow, that is, the water, oil and gas flows, obtained in 3.1;
- The axial velocity and head loss of the flow over the entire length of completions, obtained in 3.1;
- The physical dimensions of the piping in each region of the system, obtained in 3.1;
- The temperature, pressure, and phase compositions of the well in an equipment that composes the completion, obtained in 3.2.

3. RESULTS AND DISCUSSION

In this section, we present and discuss the results for the PACS-type completion with a perforated tube shown in Figure 1 (a) following the steps discussed in the methodology. Section 3.1 provides an overview of the main fluid dynamic characteristics obtained with CFD simulation in the scenario outlined in Table 4. Section 3.2 presents the results of the thermodynamic equilibrium and population balance simulations for the standard condition detailed in Table 1, while Section 3.3 explores the impact of varying water chemical compositions on the results.

3.1 CFD results

As mentioned previously, the perforated liner spreads across nearly all the extension of the open-hole completion, with each ½" hole delivering a fraction of the total well production output. In the present work, it is considered four locations for the placement of the elementary volume, as discussed over Figure 1 (a). Figure 3 displays the results for the simulation of the perforated liner, considering the simulation domain showed in Figure 2 (e). It also shows the area-averaged differential pressure between the well wall and the outlet Δp_{an} [Pa], and also the area-averaged differential pressure between the production string inlet and outlet Δp_{ps} [Pa]. In fact, the PF-bottom hole comprises just the fluid inlet area-averaged through the well wall, which then flows radially through the ½" holes and finally flow upward through the production string. In such case, the area-averaged pressure differential between the well wall and the outlet is 434 Pa. As the perforated linear is placed downstream (less deep), the maximum velocity inside the production string increases, indicating also an increase in Δp_{ps} as a higher volume of flow flows upward. As a matter of fact, Δp_{an} also have to increase to compensate the increment in Δp_{ps} and keep flow rate in each ½" hole uniform.

	PF-bottom hole	PF-inferior	PF-intermediate	PF-superior
	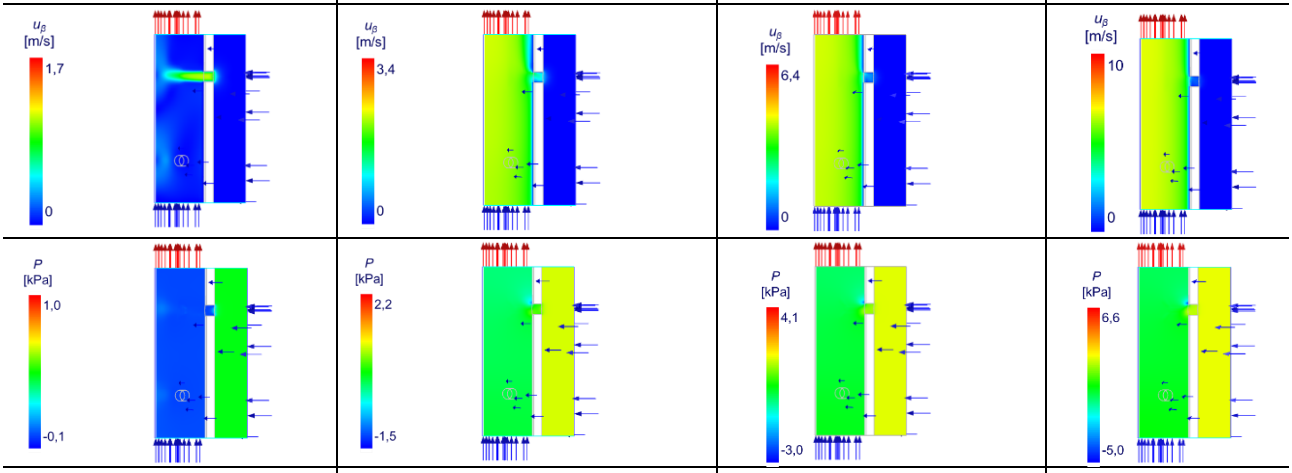			
Δp_{an}	434 Pa	970 Pa	1801 Pa	2931 Pa
Δp_{ps}	54 Pa	194 Pa	427 Pa	760 Pa

Figure 3 – Velocity magnitude and pressure fields as a function of perforated liner placement in the open-hole PACS completion.

The CFD results shown in Figure 4 (a) indicated by the triangles represent the area-averaged pressure difference between the production string inlet and outlet Δp_{ps}, also listed in Figure 3, as a function of the perforated liner depth. Notably, there is a linear-like trend between the inferior and the superior, suggesting that a linear fit represents the pressure profile all across the open-hole completion. Indeed, the pressure difference between PF-bottom hole and PF-inferior is slightly lower because the flow is not fully turbulent, but a piece-wise linear fit, represented by the line, is then applied to reach a reasonable representation for the pressure behavior all across the open-hole completion. Figure 4 (b) shows results in terms of the area-averaged velocity through the production string, also indicating that a linear fit works well.

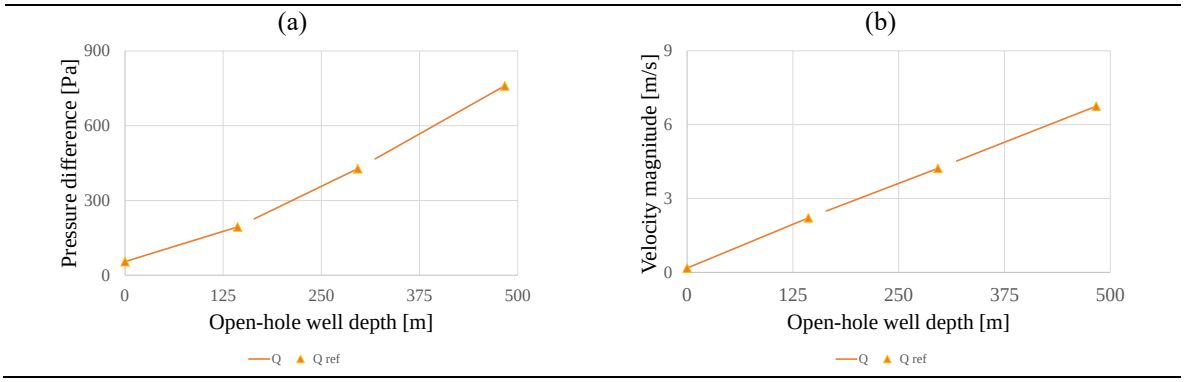

Figure 4 – Open-hole profiles for PACS 3A completion with perforated liner conceding the flow output scenarios of Table 4: (a) pressure profile; (b) velocity magnitude profile.

3.2 Thermodynamic and kinetic results – standard conditions

Table 6 displays the calculated thermodynamic potential, measured in kg/day, at the inlet and outlet of each zone in the PACS-type completion with a perforated tube. For each zone, half of the holed pipe serves as the input, while the other half serves as the output, and the production through the holes is included in each volume calculated for these regions. As shown in the table, both the inlet and outlet potentials increased with the zone sequence. This increase occurs due to the pressure drop experienced by the fluid as it flows through the productive flow that connects the zones. It was possible to observe that the fluid in the upper and intermediate regions had pressures 5.47% and 2.63% lower, on average, than those in the inferior zone; and, consequently, 3.32% and 1.57% lower carbon dioxide content in water, resulting in higher supersaturations, as per Equation 1, and thermodynamic potentials.

Table 6 – Thermodynamic potentials and crystalline production (kinetics simulation) along tree-zone open-hole completion with PACS 3A configuration with the conditions listed in Table 5.

	Thermodynamic potential		**Crystalline production**	
Zone	**Input [kg/day]**	**Output [kg/day]**	**Input [kg/day]**	**Output [kg/day]**
Superior	24.20	27.74	Superior	4.10×10^{-4}
Intermediate	17.18	20.10	Intermediate	1.13×10^{-4}
Inferior	10.09	13.87	Inferior	3.25×10^{-5}

Once the thermodynamic equilibrium distance has been calculated, it was possible to carry out kinetic simulations, which determines the crystalline concentration profile along the axial distance of the pipe and over time illustrated in Figure 5.

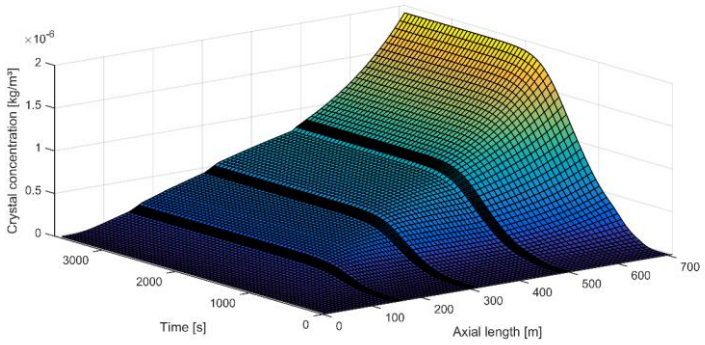

Figure 5 – Crystalline production along the tube axial length and time of operation.

Based on the kinetic profile of the completion, Table 6 was produced to present the kinetic production per zone at both the inlet and outlet in kg/day, obtained by multiplying the concentration from Figure 5 with the aqueous flow of each zone. As observed in Table 6, crystalline production increases with the sequence of zones in the PACS completion. The lower zone produces what feeds the production of the zones above, for both input and output, and the population of crystals grows and develops along the productive flow, resulting in increased crystalline mass production. Additionally, there is a mixing, every 3.5 m of the fluids produced by the holes with those inside the pipeline.

It is important to evaluate the discrepancy between the two types of output generated by the model presented in Table 6: the thermodynamic potential for CaCO3 formation, and the mass that is kinetically formed during the flow within the completion zones. The values obtained through thermodynamic calculations assume equilibrium and inform the total amount of calcium carbonate that must precipitate for the system to reach a new equilibrium without considering the time required to reach this state.

On the other hand, kinetic values can consider the time the system has to produce these solids, which is essential for a flowing system like the one presented in this case study. Thus, the difference obtained in Table 6 is directly related to the fact that the fluid has significantly shorter residence times, representing less than 1% for all zones, of the time required for thermodynamic equilibrium. Therefore, it can be concluded that the system is far from equilibrium and its associated crystalline production as the chemical equilibrium was not reached under these flow conditions. The introduction of kinetic components was necessary for a simulator to recognize the different conditions of this process and the actual crystalline production, rather than just the potential production.

The short residence times observed in all zones of the completion (66.14, 31.64, and 24.74 s for the inferior, intermediate, and superior regions, respectively) also had a significant impact on the polymorphic transformation. Despite the thermodynamic model indicating calcite as the most stable polymorph under the studied conditions, it represented only 0.92% of the total crystalline mass on average. Therefore, it is crucial to differentiate the kinetic behavior of the system in addition to the thermodynamic study. While thermodynamics indicates which crystal is the most stable and the order of their appearance, kinetics can determine the speed at which these events occur.

3.3 Thermodynamic and kinetic results – varying both temperature and pressure of operation

In this phase of the simulations, the temperature and pressure of the reservoir calculated were changed to 380.5 atm and 62ºC. This change in reservoir pressure and temperature required the adjustment of water for the system to be in thermodynamic equilibrium under the new reservoir conditions. Table 7 presents the condition of water, temperature, and pressure at the point where the flow was assumed to begin, as a result of recalculating the water and using the new temperatures and pressures in the thermodynamic and kinetic calculations in this section.

Table 7 – New conditions calculated to the variation of the reservoir temperature and pressure.

Sodium [ppm]	41.968	Sulfate [ppm]	95
Potassium [ppm]	1.751	Bicarbonate [ppm]	1.986
Magnesium[ppm]	715	pH	4,9
Calcium [ppm]	4.390	mol CO_2 [%]	16
Barium [ppm]	33	Temperature [ºC]	62
Chloride [ppm]	1.360	Pressure [bar]	380.5
Bromide [ppm]	75.902		

Based on the calculations using Table 7 conditions, the thermodynamic potential of formation for each zone in the PACS completion can be determined.
Table 8 presents these potentials, expressed in kg/day, at both the entrance and exit of each zone. Similar to Table 6, it can be observed that the thermodynamic potential increases with the sequence of zones, for both the inlet and outlet. This trend was also since the fluid in the upper and intermediate regions has pressures that are 6.13% and 2.87% respectively lower than the fluid in the lower zone. As a result, these regions exhibit greater supersaturation and thermodynamic potential. It was also possible to notice that

Table 8 presented 67.10%, 42.62% and 30.14% higher thermodynamic potential than those of Table 6. This was observed to be attributed to fact that 8.43% smaller pressure at the completion entrance, which produced 10.5%,8.6% and 7.8% smaller pressures within the production zones, was sufficient to increase the supersaturation even with the decrease of the temperature and the bicarbonate content.

Table 8 – Thermodynamic potentials and crystalline production (kinetics simulation) along tree-zone open-hole completion with PACS 3A with the conditions listed in Table 7

	Thermodynamic potential		**Crystalline production**	
Zone	**Input [kg/day]**	**Output [kg/day]**	**Input [kg/day]**	**Output [kg/day]**
Superior	32.01	35.51	1.54×10^{-4}	4.67×10^{-4}
Intermediate	25.13	27.93	7.79×10^{-5}	1.24×10^{-4}
Inferior	18.22	21.31	8.91×10^{-6}	4.84×10^{-5}

With the distance to thermodynamic equilibrium calculated, kinetic simulations can be performed, with the crystalline concentration profile along the axial distance of the pipe and time, being shown in Figure 6.

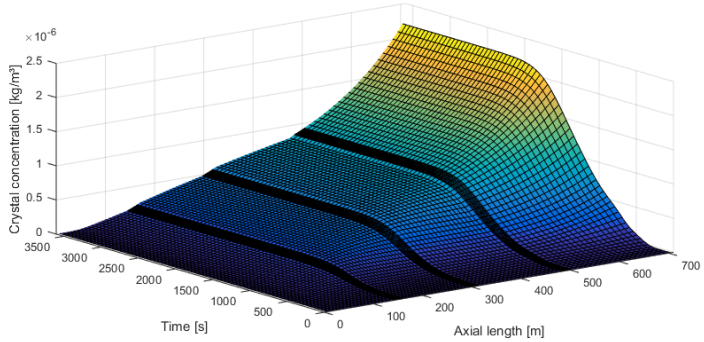

Figure 6 – Crystalline production along the tube axial length and time of operation for the modified conditions

From the kinetic profile throughout the completion, it is possible to present the kinetic production per zone, both at the inlet and outlet, in kg/day from the multiplication of the concentration obtained in Figure 6 with the aqueous flow of each zone listed in Table 3. In Table 8 is possible to observe the increase in the mass of crystals produced along the producing zones. Again, it is highlighted that in this completion all regions are directly connected; with the bottom output feeding the middle input and so on. The kinetic results followed the trend observed in the thermodynamic ones, with the production in Table 8 being higher than those of Table 6; this can be associated with higher supersaturation; thus, the particles were dispersed and produced in a medium more favorable to the precipitation with faster kinetic rates, 21.15% in average for the nucleation and growth rates, even with lower temperatures and fewer bicarbonate molecules.

4. CONCLUSIONS

This work presented one approach to characterizing the calcium carbonate kinetic formation during oil production using information on fluid dynamics and population modeling. The methodology presents a robust alternative for evaluating the criticality of various equipment designs and operating conditions within the oil industry.

By comparing the values obtained along the PACS completion, the differences that each equipment zone causes in the thermodynamics and kinetics of calcium carbonate can be evaluated. Tables 3.4 and 3.11 present the values obtained for the thermodynamic potential at the exit of the inferior, intermediate, and superior zones for the PACS completion in standard and modified conditions. It is evident that the thermodynamic potential of formation increased along the zones, due to the pressure drop along the flow, which favored the $CaCO_3$ formation reaction by releasing carbon dioxide to the gas phase. Furthermore, the condition with lower initial temperature and pressure had a higher production potential.

Using the results from the thermodynamic calculations, kinetic simulations were carried out along with the productive flow of the studied completion. Tables 3.5 and 3.12 show that crystalline production increased along the zones due to the particles produced in a lower region being carried to the new zone and continuing to develop their kinetic rates of nucleation, growth, agglomeration, and polymorphic transformation. The residence time of the particles within the completions proved to be of fundamental importance in the population kinetics, with the kinetic results presenting values in the range of mg/day against the production of kg/day obtained in thermodynamics due to the lack of time that the system had to develop until the chemical equilibrium. Again, the system with lower pressure and temperature had higher productions, this time kinetic, along the studied zones.

Therefore, the tool proposed in this work was able to carry out simulations in three different and important aspects of crystalline formation along equipment in the production of oil and gas, demonstrating interesting potential for application as a virtual salt formation sensor and even aid in the analysis and selection of equipment and compositions that may help in mitigating the formation of CaCO3. From these initial results, the CFD and kinetic models will be simulated in different completions and compositions of the phases to capture the effect that different compositions of equipment can cause in the fluid dynamic, thermodynamic, and kinetic profiles.

5. REFERENCES

Blue, C. R., Giuffre, A., Mergelsberg, S., Han, N., De Yoreo, J. J., & Dove, P. M. (2017). Chemical and physical controls on the transformation of amorphous calcium carbonate into crystalline CaCO3 polymorphs. *Geochimica et Cosmochimica Acta*, *196*, 179–196. https://doi.org/10.1016/j.gca.2016.09.004

Bouamra, R., Carneiro, G., Machado, P., da Silva, M. F., Franquiz, G., Guan, H., & Lindvig, T. (2020). Scaleprotect - Scale deposition modeling in pre-salt reservoir. *Offshore Technology Conference Brasil 2019, OTCB 2019*, 1–15. https://doi.org/10.4043/29886-ms

Brečević, L., & Kralj, D. (2008). ChemInform Abstract: On Calcium Carbonates: From Fundamental Research to Application. *ChemInform*, *39*(5), 467–484. https://doi.org/10.1002/chin.200805226

Cosmo, R. D. P. (2013). *Modelagem e Simulação Termodinâmica da Precipitação de Calcita em Condições de Poço*. Universidade Federal do Espírito Santo,Centro Universitário Norte.

Donnet, M., Bowen, P., & Lemaître, J. (2009). A thermodynamic solution model for calcium carbonate: Towards an understanding of multi-equilibria precipitation pathways. *Journal of Colloid and Interface Science*, *340*(2), 218–224. https://doi.org/10.1016/j.jcis.2009.09.005

Du, H., & Amstad, E. (2019). Water: How Does It Influence the CaCO3 Formation? *Angewandte Chemie - International Edition*. https://doi.org/10.1002/anie.201903662

Expro Petrotech. (2023, April 13). *MULTISCALE: A computer programme for prediction of mineral deposits*. Https://Www.Multiscale.No/.

Gebauer, D., Raiteri, P., Gale, J. D., & Cölfen, H. (2018). On classical and non-classical views on nucleation. *American Journal of Science*, *318*(9), 969–988. https://doi.org/10.2475/09.2018.05

Haarberg, T., Selm, I., & et al. (1992). SPE 19449 Scale Formation in Reservoir and Production Equipment During Oil Recovery : An Equilibrium Model. *Society of Petroleum Engineers*, *February*, 75–84.

Hamid, S., De Jesus, O., Jacinto, C., Izetti, R., Pinto, H., Droguett, E., Edwards, C., Cassidy, J., Zhang, H., Dagenais, P., & Batocchio, M. (2013). A Practical Method of Predicting Chemical Scale Formation in Well Completions. *SPE Saudi Arabia Section Annual Technical Symposium and Exhibition*, 19–22.

Kamal, M. S., Hussein, I., Mahmoud, M., Sultan, A. S., & Saad, M. A. S. (2018). Oilfield scale formation and chemical removal: A review. *Journal of Petroleum Science and Engineering*, *171*(July), 127–139. https://doi.org/10.1016/j.petrol.2018.07.037

Kawano, J., Shimobayashi, N., Miyake, A., & Kitamura, M. (2009). Precipitation diagram of calcium carbonate polymorphs: Its construction and significance. *Journal of Physics Condensed Matter*, *21*(42). https://doi.org/10.1088/0953-8984/21/42/425102

Lassin, A., André, L., Devau, N., Lach, A., Beuvier, T., Gibaud, A., Gaboreau, S., & Azaroual, M. (2018). Dynamics of calcium carbonate formation: Geochemical modeling of a two-step mechanism. *Geochimica et Cosmochimica Acta*, *240*, 236–254. https://doi.org/10.1016/j.gca.2018.08.033

Mayorga, I. C., Astilleros, J. M., & Fernández-Díaz, L. (2019). Precipitation of caco 3 polymorphs from aqueous solutions: The role of ph and sulphate groups. *Minerals*, *9*(3), 1–16. https://doi.org/10.3390/min9030178

Molnár, Z., Dódony, I., & Pósfai, M. (2023). Transformation of amorphous calcium carbonate in the presence of magnesium, phosphate, and mineral surfaces. *Geochimica et Cosmochimica Acta*, *345*, 90–101. https://doi.org/10.1016/j.gca.2023.01.028

Myasnikov, S. K., Chipryakova, A. P., & Kulov, N. N. (2013). Kinetics, energy characteristics, and intensification of crystallization processes in chemical precipitation of hardness ions. *Theoretical Foundations of Chemical Engineering*, *47*(5), 505–523. https://doi.org/10.1134/S0040579513050229

Neubauer, T. M. (2022). *Crystallization of calcium carbonate: Modelling thermodynamic equilibrium, pathway, nucleation, growth, agglomeration, and dissolution kinetics for the calcium carbonate polymorphs formation.* [Thesis]. UFSC.

Neubauer, T., Santos Serpa, F., Franceschi, E., Dariva, C., Sayer, C., Hermes De Araújo, P. H., Barbosa Castro, B., Aldeia, W., & Da Costa, C. (2022). Crystallization of Calcium Carbonate: Modeling Thermodynamic Equilibrium, Pathway, Nucleation, Growth, Agglomeration, and Dissolution Kinetics with the Presence of Mg2+, Ba2+, and Sr2+. *Industrial and Engineering Chemistry Research*, *61*(37), 13944–13961. https://doi.org/10.1021/acs.iecr.2c01553

Olajire, A. A. (2015). A review of oilfield scale management technology for oil and gas production. *Journal of Petroleum Science and Engineering*, *135*, 723–737. https://doi.org/10.1016/j.petrol.2015.09.011

Sanjiv Raj, K., Devi, N., & Subramanian, V. K. (2020). Effect of barium and strontium ions on the morphology and polymorphism of CaCO3. *Chemical Physics Letters*, *750*(January). https://doi.org/10.1016/j.cplett.2020.137502

Sanni, O., Kabir Raheem, Neville, A., & Charpentier, T. (2022). *Surface Precipitation and Growth Kinetics of Calcium Carbonate (CaCO3) Scale Using a Novel Capillary Flow Rig*. *August*, 1–23.

Shih, T.-H., Liou, W., Shabbir, A., Yang, Z., & Zhu, J. (1995). A new k-ε eddy viscosity model for high Reynolds number turbulent flows. *Computer Fluids*, *24*(3), 227–238. https://doi.org/https://doi.org/10.1016/0045-7930(94)00032-T

Taylor, G. I. (1932). The Viscosity of a Fluid Containing Small Drops of Another Fluid Author (s): G . I . Taylor Source : Proceedings of the Royal Society of London . Series A , Containing Papers of a Published by : Royal Society Stable URL : http://www.jstor.org/stable/960. *Proc. R. Soc. Lond. A*, *138*(834), 41–48.

U.S Geological Survey. (2023, April 13). *PHREEQC: A computer program designed to perform aqueous geochemical calculations*. Https://Www.Usgs.Gov/Software/Phreeqc-Version-3.

Van Driessche, A. E. S., Kellermeier, M., Benning, L. G., & Gebauer, D. (2017). New Perspectives and Growth Nucleation on Mineral. From Solutions Precursors to Solid Materials. In *Springer*. https://doi.org/10.1007/978-3-319-45669-0_3

6. RESPONSIBILITY NOTICE

The authors are the only responsible for the printed material included in this paper.